引用格式：LI Yangjin, FAN Xian, LONG Guanfu, et al. Spatter Dynamic Recognition and Feature Analysis During High-power Disk Laser Welding[J]. Acta Photonica Sinica, 2021, 50(2):0214002
黎扬进,范西岸,龙观富,等.大功率盘形激光焊接飞溅动态识别和特征分析[J].光子学报,2021,50(2):0214002

大功率盘形激光焊接飞溅动态识别和特征分析

黎扬进[1],范西岸[1],龙观富[1],张南峰[1,2],张艳喜[1],游德勇[1],高向东[1]
(1 广东工业大学 广东省焊接工程技术研究中心,广州 510006)
(2 黄埔海关技术中心,广东 东莞 523076)

摘 要:提出了一种识别飞溅动态并基于飞溅特征分析焊接状态的方法。以304不锈钢板为试验对象,进行大功率盘形激光平板堆焊试验。利用高速相机捕捉紫外波段和可见光波段的飞溅图像,通过图像处理提取飞溅特征参数,包括质心位置、面积、灰度、平均灰度和半径。基于飞溅特征参数建立飞溅搜索信息库和相似度函数,用于识别飞溅、计算飞溅体积和灰度以及评估焊接状态。通过焊缝宽度与飞溅特征信息的比较,研究焊接状态与飞溅特征参数之间的内在关系。对飞溅特征与焊接状态之间关系进行了试验分析,结果表明,激光焊接过程中飞溅的体积和灰度值增大,焊缝宽度会相应减小,通过飞溅特征参数可有效监测和评估大功率盘形激光焊接过程的状态。

关键词:焊接工艺与设备;飞溅动态识别;激光焊接;相似度函数;特征提取;自动识别;图像处理;模式识别
中图分类号:TG409 **文献标识码**:A **doi**:10.3788/gzxb20215002.0214002

Spatter Dynamic Recognition and Feature Analysis During High-power Disk Laser Welding

LI Yangjin[1], FAN Xian[1], LONG Guanfu[1], ZHANG Nanfeng[1,2], ZHANG Yanxi[1], YOU Deyong[1], GAO Xiangdong[1]
(1 *Guangdong Provincial Welding Engineering Technology Research Center, Guangdong University of Technology, Guangzhou* 510006, *China*)
(2 *Huangpu Customs Technical Center, Dongguan, Guangdong* 523076, *China*)

Abstract: An approach for recognizing spatter dynamics and analyzing welding status based on spatter feature is proposed. A type 304 austenitic stainless steel plate is taken as a testing object for high-power disk laser bead-on-plate welding experiment. A high-speed camera is used to capture the ultraviolet band and visible light band spatter images. Image processing extracted spatter feature parameters, including centroid position, area, grayscale, average grayscale, and radius. Spatter searching information database and similarity functions are established based on spatter feature parameters to recognize the spatter, calculate spatter volume and grayscale, and evaluate the welding status. By comparing the weld seam width with the spatter feature information, the internal relation between the welding status and the spatter feature parameters is investigated. The test results of the relationship between spatter characteristics and welding state show that the weld width will decrease with the increase of spatter volume and gray value in the

Foundation item: National Natural Science Foundation of China (No.51805090), Guangzhou Municipal Special Fund Project for Scientific and Technological Innovation and Development (Nos.202002020068, 202002030147)
First author: LI Yangjin(1995—), male, M.S. degree camdidate, mainly focuses on automatic welding. Email: liyangjin99@163.com
Supervisor(Contact author): GAO Xiangdong(1963—), male, professor, Ph. D. degree, mainly focuses on welding automation. Email: gaoxd666@126.com
Received: Jun.24,2020; **Accepted**: Nov.4,2020

process of laser welding. It can be seen that the status of a high-power disk laser welding process could be monitored and evaluated through the spatter feature parameters.

Key words: Welding process and equipment; Spatter dynamic recognition; Laser welding; Similarity functions; Feature extraction; Automatic identification; Image Processing; Pattern recognition

OCIS Codes: 140.0140; 110.0110; 040.7190

0 Introduction

With fast heating process, minimal distortion by heat and great heat concentration, laser is one of the advanced machining technologies[1-3]. Among those machining technologies, high-power disk laser welding occupies a certain market in welding industry. Estimating the weld quality in real time to maintain high productivity is necessary, so we must first find the relationship between the rules of changing sensing characteristics in welding process and the weld quality[4]. Metal spatter is one of the important phenomena during laser welding. A portion of the weldment melts and forms a molten pool and a keyhole. The molten pool and the keyhole are filled with metal vapor plume. When the metal vapor plume becomes critical, a spatter will be released from a weld pool because of the steam recoil force inside the keyhole[5-7]. A strong shear force of a laser-induced plume mainly influenced the generation of spatters that is greatly reduced by controlling the direction of the plume blowing out of a keyhole inlet[8, 9]. Spatters produced during laser welding affect the molten pool's shape and the welding quality[10, 11]. Effective monitoring and control of metal spatters is considered to be one of the prerequisites to perform high-quality welding.

Many monitoring methods estimate weld quality, such as acoustic emission, optical signal, and temperature field evolution[12, 13]. The study of high-power disk laser welding spatter mainly concentrates on the microstructure of spatter, spatter eruption status, and weldments pollution and analyzes the welding status by changing the high-power disk laser welding conditions[14-16]. The optical monitoring of the weld pool and the surrounding area via a high-frame-rate camera measures and classifies the spatter in gas arc welding to investigate the relationship between workpiece contamination and weld spatter[17]. The different types of spatter phenomena occurring during laser welding are depicted with a categorization system that is proposed to facilitate the comparison and combination of research findings on spatter[18]. The Ultraviolet (UV) and Infrared (IR) sensors were used to collect plasma and spatter signals during welding and were analyzed by multiple characteristics of pattern recognition to evaluate welding quality. Kalman filter and pattern recognition algorithm were adopted to improve the accuracy rate of spatter recognition and the effectiveness of spatter feature analysis[19]. The spatter motion features were investigated using motion tracking method[20]. It was possible that the welding spatter position was accurately calculated by using image recognition technology, thus eliminating the spatter influence on molten pool recognition[21]. Also, spatter detection could be realized by using a monitoring system for laser beam welding based on Neural Network (NN) algorithm[21, 22]. This paper proposes a new method to recognize the spatters by using spatter searching information database and similarity functions.

A type 304 austenitic stainless steel plate is taken as the testing object for the high-power disk laser bead-on-plate welding experiment. To extract instantaneous variation information of metal spatters to analyze spatter feature better, a high-speed camera is used to capture the ultraviolet band and visible light band spatter images of welding. Spatter feature parameters including centroid position, area, grayscale, average grayscale, and radius are extracted from each image after preprocessing. Spatter searching information database and similarity functions are established based on the spatter feature parameters. The spatters produced during and before time t could be distinguished by comparing the spatter similarity functions. The radius calculated the volume of the spatters produced at time t. The statistic of the volume and grayscale of the spatters of different welding areas, the proportion under different threshold, and the change of the weld seam width evaluated the welding quality.

1 Experimental setup

The experiment consists of a high-power disk laser TruDisk-10003 (10 kW), a Motoman 6-axis robot, a welding experimental platform, an NAC high-speed camera (2 000 f/s), a shielding gas (argon), and a type 304 austenitic stainless workpiece (150 mm×100 mm×20 mm). The diameter of the laser spot is 480 μm, the

wavelength of the laser is 1 030 nm, and the welding speed is 4.5 m/min. The spectral band of the high-speed camera is 320～750 nm (ultraviolet + invisible light)[23]. An image recorder stores the spatter images (512 pixel×512 pixel). A precise servomotor is installed on the experimental platform drives the workpiece. The whole experiment system is shown in Fig. 1.

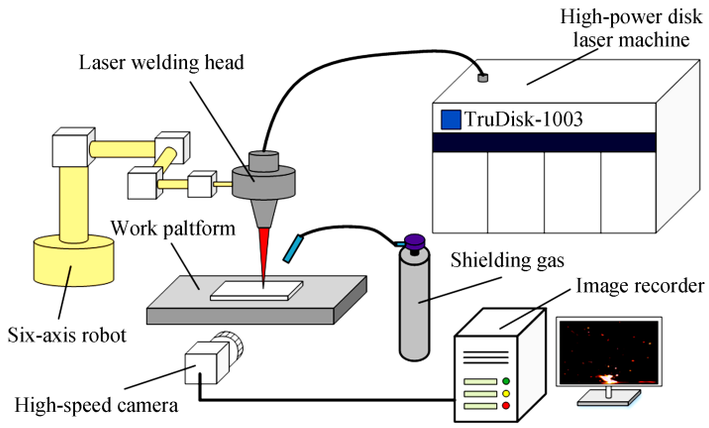

Fig. 1 High-power disk laser bead on plate welding

2 Spatter dynamic recognition

2.1 Main idea of dynamic recognition algorithm

After image preprocessing, the movement of the spatter could be estimated by comparing the spatter features of adjacent time in successive images. The continuous eight-image sequence is shown in Fig. 2. The

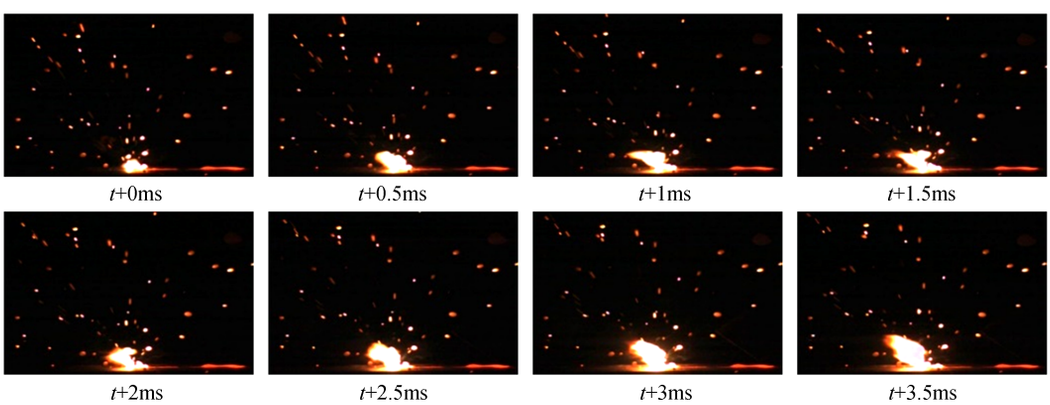

Fig. 2 Eight frames of consecutive spatter images

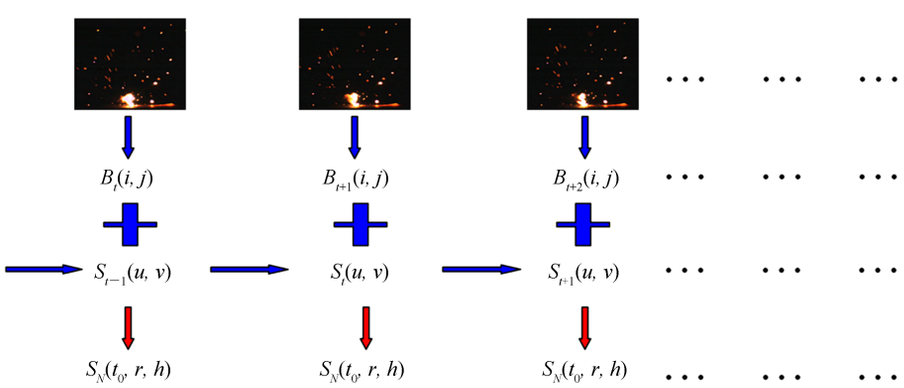

Fig. 3 Schematic diagram of spatter recognition

schematic diagram of spatter recognition tracking is shown in Fig. 3. First, the spatter feature information of image I_t for each time t is calculated and stored in $B_t(i,j)$. Second, the new spatters of I_t is distinguished by comparing the differences of spatter feature information between $B_t(i,j)$ and the searching information database $S_t(u,v)$. Finally, the information of these new spatters is saved into the new spatter database $S_N(t,r,h)$, and the corresponding values of the spatters in $S_t(u,v)$ are updated[23].

2.2 Definition of spatter features

All spatter feature information of I_t at time t is stored in $B_t(i,j)$. To obtain accurate spatter features and eliminate metal plumes, the spatter images are preprocessed[23]. The information of a spatter of image I is stored in $B_t(i,j)$, which contained six characteristics of spatter j at time t. The six characteristics are centroid abscissa $B_t(1,j)$, centroid ordinate $B_t(2,j)$, area $B_t(3,j)$, grayscale $B_t(4,j)$, average grayscale $B_t(5,j)$, and radius $B_t(6,j)$. They are defined as

$$B_t(1,j)=\frac{\sum\limits_{x,y\in D_t(j)} I_t(x,y)\times x}{\sum\limits_{x,y\in D_t(j)} I_t(x,y)} \quad x,y=1,\cdots,512 \tag{1}$$

$$B_t(2,j)=\frac{\sum\limits_{x,y\in D_t(j)} I_t(x,y)\times y}{\sum\limits_{x,y\in D_t(j)} I_t(x,y)} \quad x,y=1,\cdots,512 \tag{2}$$

$$B_t(3,j)=d_t(j) \quad x,y=1,\cdots,512 \tag{3}$$

$$B_t(4,j)=\sum_{x,y\in D_t(j)} I_t(x,y) \quad x,y=1,\cdots,512 \tag{4}$$

$$B_t(5,j)=\frac{\sum\limits_{x,y\in D_t(j)} I_t(x,y)}{d_t(j)} \quad x,y=1,\cdots,512 \tag{5}$$

$$B_t(6,j)=\min_{x,y\in E_t(j)}\sqrt{[x-B_t(1,j)]^2+[y-B_t(2,j)]^2} \quad x,y=1,\cdots,512 \tag{6}$$

where $I_t(x,y)$ is the grayscale of pixel (x,y) of spatter image I at time t, $D_t(j)$ represents the covering area of spatter j at time t, $d_t(j)$ represents the pixel numbers of the covering area of spatter j at time t, and $E_t(j)$ represents the edge of the covering area of spatter j at time t.

A residual of the peripheral vision of moving spatters is collected in the experiment because of the camera"s high-speed shooting (2 000 f/s). The spatters detected in the spatter image are mainly round and rod shaped. But the original entity of the spatter is similar to a sphere. The spatter radius is the minimum distance of the edge to the centroid of the spatter, as shown in Fig. 4. The red line is the shape of the spatter detected in the spatter image. The yellow line is the original entity shape of the spatter, and the blue line is the spatter radius.

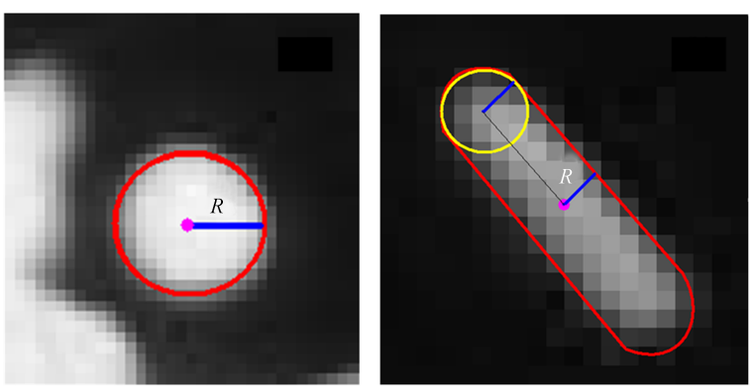

(a) Round-shaped spatter (b) Rod-shaped spatter

Fig. 4 Definition of spatter radius

2.3 Creation of spatter searching information database

To recognize the spatter produced at time t, the spatter searching information database $S_t(u,v)$ and similarity functions are established. Table 1 lists the information of $S_t(u,v)$, where $u=1,\cdots,20$ and v is the number of spatters. The information for each spatter detected for the first time is saved into $S_t(u,v)$, defined as the initial spatter information, and is then replaced with new information if another one is detected. The current information keeps on updating until the spatter disappears[23].

Table 1 Information of spatter searching data-base

u	Searching information database $S_t(u,v)$
1	Centroid abscissa x of initial spatter
2	Centroid ordinate y of initial spatter
3	Centroid ordinate y of initial spatter
4	Grayscale of initial spatter
5	Average grayscale of initial spatter
6	Radius of initial spatter
7	Speed of initial spatter
8	Variation of centroid abscissa x
9	Variation of centroid ordinate y
10	Number of initial spatter image frames
11	Centroid abscissa x of current spatter
12	Centroid ordinate y of current spatter
13	Area of current spatter
14	Grayscale of current spatter
15	Average grayscale of current spatter
16	Radius of current spatter
17	Speed of current spatter
18	Direction of spatter
19	Number of times the spatter appeared
20	Number of times the spatter disappeared

The spatter feature information of the I_t is calculated and stored in the $B_t(i,j)$ by detecting the spatters in a continuous image sequence. Then the new spatters of I_t are distinguished by comparing the different spatter feature information of $B_t(i,j)$ and $S_t(u,v)$. The information of these new spatters in the searching information database $S_t(u,v)$ is updated to recognize the new spatters.

2.4 Calculation of spatter direction and searching region

Spatters are distributed in different areas in the welding image because it erupts toward different directions in laser welding. Some spatters fall from the top of the shooting area. Therefore, different calculations of the direction angle should be considered[23], as shown in Fig. 5.

The a_x, a_y, and the angle θ of spatter direction in Fig. 5 are defined as

$$a_x = B_t(1,j) - S_{t-1}(11,v) \tag{7}$$

$$a_y = B_t(2,j) - S_{t-1}(12,v) \tag{8}$$

If $a_x \leqslant 0$, namely $\theta \in (-\frac{\pi}{2}, \frac{\pi}{2})$,

$$\theta = \arcsin\left(\frac{a_y}{\sqrt{{a_x}^2 + {a_y}^2}}\right) \tag{9}$$

If $a_x \geqslant 0$ & $a_y \geqslant 0$, namely $\theta \in (\frac{\pi}{2}, \pi)$,

$$\theta = \pi - \arcsin\left(\frac{a_y}{\sqrt{{a_x}^2 + {a_y}^2}}\right) \tag{10}$$

If $a_x \geqslant 0$ & $a_y < 0$, namely $\theta \in (-\pi, -\frac{\pi}{2})$,

$$\theta = -\pi - \arcsin\left(\frac{a_y}{\sqrt{{a_x}^2 + {a_y}^2}}\right) \tag{11}$$

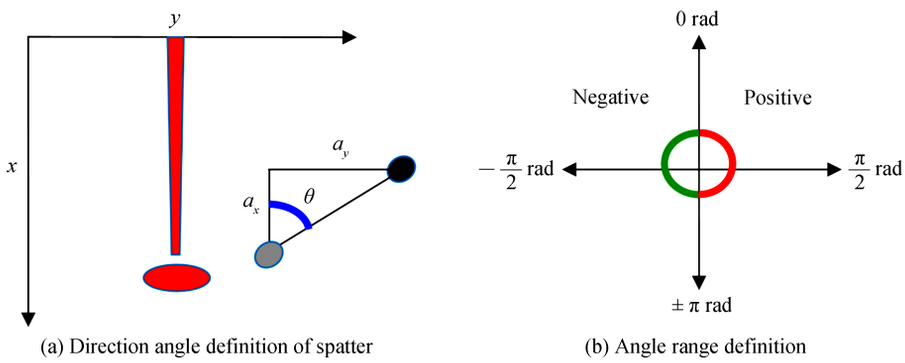

Fig. 5 Definition of spatter direction

To improve the recognition efficiency and accuracy, the spatter velocity and direction are used to calculate the spatter searching region. Spatter moving distance L is defined as the product of spatter velocity and moving time t (adjacent to image time interval 0.5 ms). The spatter searching region is a rectangle whose side length is 12 pixels larger than L in the axis projection, as shown in Fig. 6. If the velocity is zero, the searching region is a square with the spatter centroid as the center, whose side length is 60 pixels.

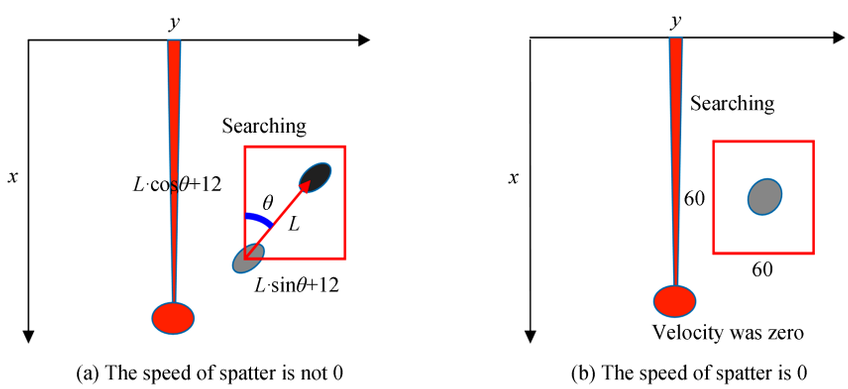

Fig. 6 Definition of searching region

2.5 Establishment of spatter similarity function and dynamic recognition algorithm

To determine whether the spatters in different images are new or old, the spatter shape similarity function $f_s(j, v)$ is established based on spatter area, grayscale, and average grayscale. The angle similarity function $f_a(j, v)$ is established based on spatter direction angle θ. Their computational formulas are shown as[23]

$$f_a(j, v) = \left|\theta - S_{t-1}(18, v)\right| \tag{12}$$

$$f_s(j, v) = \frac{\left|B_t(3, j) - S_{t-1}(13, v)\right|}{S_{t-1}(13, v)} + \frac{\left|B_t(4, j) - S_{t-1}(14, v)\right|}{S_{t-1}(14, v)} + \frac{\left|B_t(5, j) - S_{t-1}(15, v)\right|}{S_{t-1}(15, v)} \tag{13}$$

where θ is the spatter direction angle.

The new position and feature parameters of a spatter could be predicted by comparing the shape similarity function $f_s(j, v)$ with the angle similarity function $f_a(j, v)$ of the spatter produced prior to time t and adding its new information to the searching information database. Through experimental comparison, set threshold S of $f_s(j, v)$ to 0.4 and set threshold A of $f_a(j, v)$ to $\Pi/12$. If spatters in $S_{t-1}(u, v)$ and $B_t(i, j)$ could meet the similar condition $\min(f_s(j, v)) < S \bigcap f_a(j, v) < A$, they are considered to be the same, and the corresponding items of the spatter in the searching information database $S(u, v)$ are updated, which is shown in Eq. (14).

$S_t(8,v)$ and $S_t(9,v)$ are the variations of spatter centroid abscissa x and centroid ordinate y. There are six feature information of the current spatter from $S_t(11,v)$ to $S_t(16,v)$. $S_t(17,v)$ is the velocity of the current spatter, which is equal to distance divided by time. $S_t(18,v)$ is the spatter direction calculated by Eqs. (7)~(11). $S_t(19,v)$ represents the times that a spatter appears. It is increased when a spatter is currently detected again.

If $\min(f_s(j,v))<S\bigcap f_a(j,v)<A$,

$$\begin{cases} S_t(8,v)=B_t(1,j)-S_{t-1}(11,v) \\ S_t(9,v)=B_t(2,j)-S_{t-1}(12) \\ S_t(11,v)=B_t(1,j) \\ S_t(12,v)=B_t(2,j) \\ S_t(13,v)=B_t(3,j) \\ S_t(14,v)=B_t(4,j) \\ S_t(15,v)=B_t(5,j) \\ S_t(16,v)=B_t(6,j) \\ S_t(17,v)=\sqrt{\left[B_t(1,j)-S_{t-1}(11,v)\right]^2+\left[B_t(2,j)-S_{t-1}(12,v)\right]^2}/0.5 \\ S_t(18,v)=\theta \\ S_t(19,v)=S_{t-1}(19,v)+1 \end{cases} \tag{14}$$

If spatters in $S_{t-1}(u,v)$ and $B_t(i,j)$ could not meet the same condition, the spatter disappears or is currently overlapped by other spatters (because of the camera can only shoot two-dimensional graphics). However, it is entirely possible to occur at the next moment, so the trajectory prediction should be taken. The corresponding items of the spatter in the searching information database $S(u,v)$ are updated[23], which is shown in Eq. (15).

If $\min(f_s(j,v))>S\bigcup f_a(j,v)>A$,

$$\begin{cases} S_t(11,v)=S_{t-1}(11,v)+S_{t-1}(8,v) \\ S_t(12,v)=S_{t-1}(12,v)+S_{t-1}(9,v) \\ S_t(20,v)=S_{t-1}(20,v)+1 \end{cases} \tag{15}$$

$S_t(11,v)$ and $S_t(12,v)$ are the centroid abscissa x and centroid ordinate y, respectively. The variation of centroid coordinate is needed to calculate them since the spatter has not been detected at this time. $S_t(20,v)$ represents the times of disappearance. It increases when a spatter has currently disappeared and determines whether the spatter is new.

After the spatter searching, if spatter j in $B_t(i,j)$ is not similar to any spatter in $S_{t-1}(u,v)$, it is considered to be the first detected spatter at time t. The information $S_t(u,v+l)(l=1,\cdots,m$, where m is the number of spatters first detected at time t) is stored in the searching information database $S(u,v)$ with the corresponding initial value. The computational formulas of assignment and renewal are shown in Eq. (16). $S_t(10,v)$ means the number of initial spatter image frames, that is, the time of obtaining the initial spatter image. $S_t(19,v)$ represents the times that the spatter appeared. It is assigned as 1 since the spatter is detected first. The initial value of the rest of the spatter information in $S(u,v)$ is 0.

The spatter eruption situation is so complex that some special issues should be considered, such as the spatter appearing on the border of image and irregular metal plumes and other noise information occurring in welding. The spatter is not a new one if it appears on the border. It needs to be dealt with by setting the starting point coordinate boundary conditions, as shown in Eq. (17). Irregular metal plumes (halo) and noise information could be dealt with by setting the terminal point coordinate border conditions, which are shown in Eq. (18). If both $S_t(1,v)$ and $S_t(2,v)$ could meet the boundary conditions of the starting point coordinate, the spatter is identified as a falling spatter or interference noise rather than a new one[23]. If a spatter could meet the terminal point coordinate border conditions, the spatter has been existing in this area and is identified as a metal plume (halo) or an interference noise rather than a new spatter.

$$\begin{cases} S_t(1,v+l)=B_t(1,l) \\ S_t(2,v+l)=B_t(2,l) \\ S_t(3,v+l)=B_t(3,l) \\ S_t(4,v+l)=B_t(4,l) \\ S_t(5,v+l)=B_t(5,l) \\ S_t(7,v+l)=0 \\ S_t(8,v+l)=0 \\ S_t(9,v+l)=0 \\ S_t(10,v+l)=t \\ S_t(11,v+l)=B_t(1,l) \\ S_t(12,v+l)=B_t(2,l) \\ S_t(13,v+l)=B_t(3,l) \\ S_t(14,v+l)=B_t(4,l) \\ S_t(15,v+l)=B_t(5,l) \\ S_t(16,v+l)=B_t(6,l) \\ S_t(17,v+l)=0 \\ S_t(18,v+l)=0 \\ S_t(19,v+l)=1 \\ S_t(20,v+l)=0 \end{cases} \tag{16}$$

$$S_t(1,v)<480 \bigcap S_t(1,v)>150 \bigcap S_t(2,v)>50 \bigcap S_t(2,v)<450 \tag{17}$$

$$\begin{cases} S_{t+m}(1,v)<490 \bigcap S_{t+m}(1,v)>320 \bigcap S_{t+m}(2,v)>120 \bigcap S_{t+m}(2,v)<320 \\ S_{t+m}(11,v)<490 \bigcap S_{t+m}(11,v)>320 \bigcap S_{t+m}(12,v)>120 \bigcap S_{t+m}(12,v)<320 \end{cases} \tag{18}$$

By experimental comparison, set the spatter occurrence frequency threshold N_e to 6 to filter the noise information of spatter images. If the spatter occurrence frequency $S_t(19,v) \geqslant N_e$ with special treatment, a new spatter is produced at time t, and its information is saved to the new spatter database $S_N(t,r,h)$, where r is the number of new spatters and h is the characteristics of the new spatter. To improve the recognition efficiency and avoid spatter searching information $S(u,v)$ overloading, when spatter disappear frequency $S(20,v)$ is greater than 10, the spatter information should be removed. The flowcharts of spatter recognition algorithm and spatter recognition effect are shown in Figs. 7 and 8, respectively.

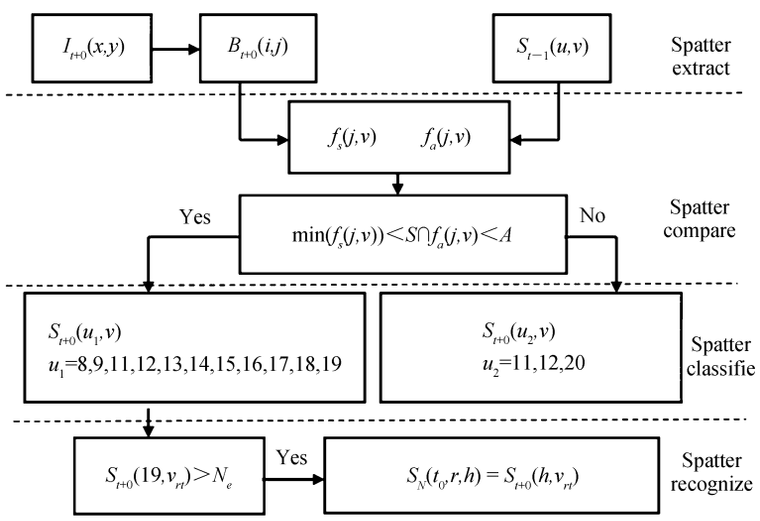

Fig. 7 Flow chart of spatter recognition algorithm

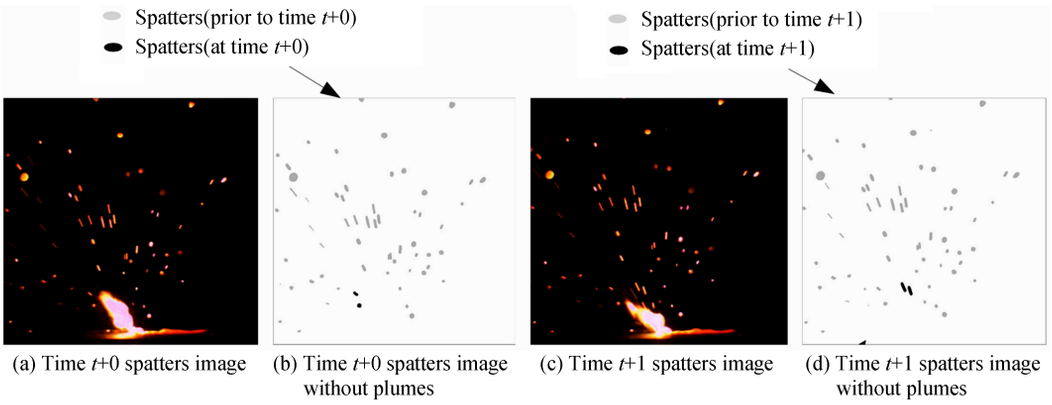

Fig. 8 Spatter recognition effect

3 Statistic analysis of spatter characteristic

Laser welding is physical reaction with dramatic changes in energy, in which the metal plumes greatly influence the laser beam by absorbing, refracting, and reflecting it. The periodic variation of metal plumes will lead to the periodic variation of absorbing the laser energy. The width of the welding seam will also change in varying degrees, so dividing the welding seam in regions to analyze the relationship between the spatter feature parameters and the welding quality better is necessary. Region division and the corresponding width of the welding seam are shown in Fig. 9.

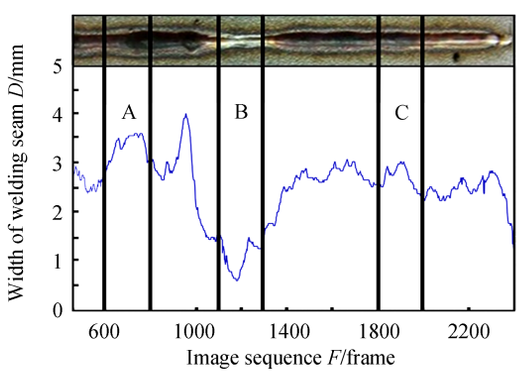

Fig. 9 Regionalism curve of weld seam width

Welding quality and stability can be reflected by the width of the welding seam, obviously, the welding seams of regions A and C are wider and more stable than that of region B. Hence, the welding quality of region B is the worst, and regions A and C seem better. The feature parameters of new spatters can be extracted after spatter dynamic recognition, such as number, radius, volume, speed, direction angle, area, and grayscale. Therefore, this test studies these three representative regions to explore the relationship between spatters and welding quality.

The sphere volume formula calculates the volume of spatters produced at time t, which is shown in Eq. (19). The volume and grayscale of new spatters are shown in Fig. 10, both of them representing the summation of all the new spatters produced at any time.

$$V(t)=\sum_{k=1}^{n}\frac{4}{3}\pi R_k^3 \quad t=1,2,\cdots,2500 \tag{19}$$

where $V(t)$ is the volume of spatters produced at time t, n is the number of spatters produced at time t and R_k is the spatter radius of the corresponding k spatter.

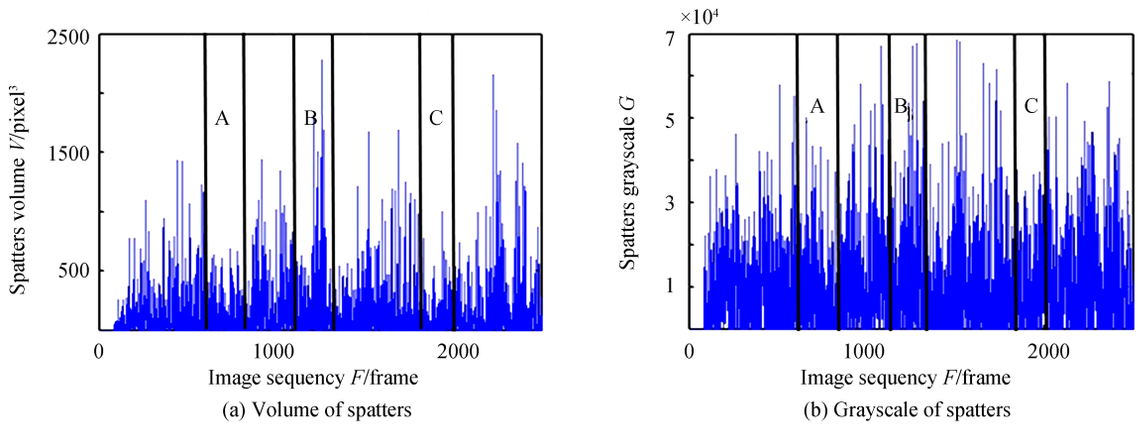

Fig. 10 Volume and grayscale of spatters

The statistics of spatter volume and grayscale for these three regions are shown in Tables 2 and 3, respectively. Both the summation and the proportion based on the different threshold of the spatter′s volume and grayscale of region B are greater than others. According to the above analysis, when the width of the weld seam suddenly becomes small, the volume and grayscale of spatter in the welding experiment will increase correspondingly. The width of weld seam usually fluctuates within a certain range. If the changing amplitude of weld width exceeds certain threshold, a poor weld formation can be determined.

Table 2 Statistic of spatter volume of A, B, C regions

Image sequence F	Spatter volume/pixel	Proportion of volume greater than 1 000	Proportion of volume greater than 500
A(601～800f)	19 482	1%	6.5%
B(1101～1300f)	32 376	3.5%	9%
C(1801～2000f)	28 580	2.5%	7.5%

Table 3 Statistic of spatter grayscale of A, B, C regions

Image sequence F	Spatter grayscale	Proportion of grayscale greater than 35 000	Proportion of grayscale greater than 20 000
A(601～800f)	1 539 800	2.5%	10.5%
B(1 101～1 300f)	2 195 000	6.5%	17.5%
C(1 801～2 000f)	1 916 100	3%	16%

4 Conclusions

The instantaneous information of spatters could be captured by using a high-speed camera during high-power disk laser welding. Experimental results showed that the spatters produced during the welding experiment could be accurately detected using the proposed spatters recognition algorithm after preprocessing. The feature parameters of the spatters could be accurately extracted and calculated. The width of region B dramatically decreased in the middle area of the welding seam. Thus, the welding quality of region B was the worst. The volume and grayscale of region B were greater than others by comparing the weld seam width with the spatter feature information, which shows that the spatter feature information and the welding quality are closely related. Under normal circumstances, the weld width would be reduced correspondingly when the volume and the grayscale of the spatter increased in the process of laser welding. Therefore, the volume and grayscale the of the spatter could be used to effectively quantify information and evaluate welding quality. They greatly reflect the real-time quality of laser welding.

Acknowledgments

Many thanks are given to Katayama Laboratory of Osaka University for their assistance of laser welding experiments.

References

[1] YANG Qibiao, ZHANG Hong, ZHOU Wei, et al. Surface incubation effect of carbide yg6 induced by femtosecond laser [J]. Acta Photonica Sinica,2019,48(6):614002.

[2] ZHANG Junzhan, ZHANG Yuanmin, LIU Yongsheng, et al. Femtosecond laser ablation properties of ZrO_2 and Al_2O_3 ceramics at linear and circular polarized light[J]. Acta Photonica Sinica, 2018,47(6):614003.

[3] SU Shi, AN Zhiyong, LIANG Wei, et al. Comparisons and analysis of drilling experiment using different pulse laser wavaforms[J]. Acta Photonica Sinica, 2012,41(5):565-570.

[4] CHANG Fei, ZHANG Jian, XIE Yunchao, et al. Fabrication, characterization, and photocatalytic performance of exfoliated g-C3N4-TiO2 hybrids[J]. Applied Surface Science, 2014, 311(9):574-581.

[5] GAO Xiangdong, ZHANG Yanxi. Monitoring of welding status by molten pool morphology during high-power disk laser welding[J]. Optik-International Journal for Light and Electron Optics, 2015,126(19):1797-1802.

[6] HEIDER A, SOLLINGER J, ABT F, et al. High-speed X-ray analysis of spatter formation in laser welding of copper[J]. Physics Procedia, 2013,41:112-118.

[7] OKAMOTO Y, YAMAMOTO H, OKADA A, et al. Velocity and angle of spatter in fine laser processing[J]. Physics Procedia, 2012,39:792-799.

[8] GAN Yu, WANG Wenxian, CUI Zeqin, et al. Numerical and experimental study of the temperature field evolution[J]. Optik-International Journal for Light and Electron Optics, 2015,126(7-8):739-743.

[9] ZHANG M J, CHEN G Y, ZHOU Y, et al. Observation of spatter formation mechanisms in high-power fiber laser welding of thick plate[J]. Applied Surface Science, 2013,280:868-875.

[10] SIMONELLI M, TUCK C, ABOULKHAIR N T, et al. A study on the laser spatter and the oxidation reactions during selective laser melting of 316l stainless steel, Al-Si_{10}-Mg, and Ti-6Al-4V[J]. Metallurgical and Materials Transactions A-Physical Metallurgy and Materials Science, 2015,46(9):3842-3851.

[11] XIA Xinmiao, JIANG Zhaoliang, XU Pengfei. A detection algorithm of spatter on welding plate surface based on machine vision[J]. Optoelectronics Letters, 2019, 15(1): 52-56 .

[12] SHCHEGLOV P Y, GUMENYUK A V, GORNUSHKIN I B, et al. Vapor - plasma plume investigation during high-power fiber laser welding[J]. Laser Physics, 2012,23(1):16001.

[13] WEI Huang, RADOVAN K. A laser-based vision system for weld quality inspection[J]. Sensors, 2011,11(1):506-521.

[14] LI Kai, GAO Hongming, LI Haichao, et al. Droplet rebounded spatter in dry hyperbaric gas metal arc welding process [J]. International Journal of Advanced Manufacturing Technology, 2014,74(5-8):693-698.

[15] SHCHEGLOV P Y, USPENSKIY S A, GUMENYUK AV, et al. Plume attenuation of laser radiation during high power fiber laser welding[J]. Laser Physics Letters, 2011,8(6):475-480.

[16] COLOMBO D, COLOSIMO B M, PREVITALI B. Comparison of methods for data analysis in the remote monitoring of remote laser welding[J]. Optics & Lasers in Engineering, 2013,51(1):34-46.

[17] CAO Bin, XIANG Yuanpeng, LV Xiaoqing, et al. Approximate entropy-a new statistic to quantify arc and welding process stability in short-circuiting gas metal arc welding[J]. Chinese Physics B, 2008,17(3):865-879.

[18] POWELL J, KAPLAN A F H. Spatter in laser welding[J]. Journal of Laser Applications, 2011,23(3):1-7.

[19] SCHWEIER M, HEINS J F, HAUBOLD M W, et al. spatter formation in laser welding with beam oscillation[J]. Physics Procedia, 2013,41:20-30.

[20] HUANG Ye, HUA Xueming, LI Fang, et al. Spatter feature analysis in laser welding based on motion tracking method [J]. Journal of Manufacturing Processes, 2020, 55:220-229.

[21] HAH M L, PULHANI A K, SURI B M, et al. Time-resolved emission spectroscopic study of laser-induced steel plasmas[J]. Plasma Science and Technology, 2013,15(6):546.

[22] GAO Xiangdong, SUN Yan, KATAYAMA S. Neural network of plume and spatter for monitoring high-power disk laser welding[J]. International Journal of Precision Engineering and Manufacturing-Green technology, 2014,1(4):293-298.

[23] LONG Guanfu. Analysis of characteristics of spatters during high-power disk laser welding[D]. Guangzhou: Guangdong University of Technology, 2012.